JOURNAL OF GEOPHYSICAL RESEARCH, VOL. 105, NO. B7, PAGES 16,683–16,697, JULY 10, 2000

Micromechanical modeling of cracking and failure in brittle rocks

James F. Hazzard and R. Paul Young
Department of Earth Sciences, University of Liverpool, Liverpool, England

S. C. Maxwell
ESG Canada Inc., Kingston, Ontario, Canada

Abstract. Dynamic micromechanical models are used to analyze crack nucleation and propagation in brittle rock. Models of rock are created by bonding together thousands of individual particles at points of contact. The feasibility of using these bonded particle models to reproduce rock mechanical behavior is explored by comparing model behavior to results from actual laboratory tests on different rock types. The behavior of two granite models are examined in detail to study cracking and failure patterns that occur during compressional loading. Because discontinuum models are being used, the rock models are free to crack and break apart under stress, such that the micromechanics of cracking can be examined. Stress waves are allowed to propagate outward from each crack, and it is shown that these dynamic waves significantly affect the rock behavior. As the peak stress in the modeled rock is approached and many of the bonds are close to breaking, a passing wave from a nearby crack is sufficient to break more bonds. This causes clusters of cracks to be created, and then eventual macroscopic shear failure occurs as these clusters connect to bisect the sample. The failure patterns observed in the granite models are similar to those observed in actual laboratory tests.

1. Introduction

Most rocks near the Earth's surface are brittle and filled with fractures, cracks, and inhomogeneities. It is the presence or creation of these discontinua that cause the rock behavior to deviate from true elastic. Knowledge of the amount, size, and geometry of these cracks and how they effect the mechanical behavior of rock (peak strength, stiffness, and permeability) is extremely important in engineering endeavors and in the understanding of geological processes. In particular, the way in which fractures form and coalesce may have importance in earthquake understanding and prediction [*Lockner*, 1995; *Scholz et al.*, 1973].

It has long been known that the strength of brittle rocks under compression depends on the growth of flaws and cracks and how these cracks propagate and coalesce into larger shear faults. Microscopic observation of stressed laboratory rock samples has shown that most cracks that form during compression are tensile and subparallel to the maximum compressive stress [*Moore and Lockner*, 1995; *Tapponnier and Brace*, 1976]. This fact is emphasized by observing that samples dilate as peak stress is approached [*Brace et al.*, 1966]. Direct observation has also shown that shear cracks cannot propagate in their own plane [*Brace and Bombolakis*, 1963; *Horii and Nemat-Nasser*, 1985]. Therefore the eventual failure of the sample must occur by interaction of the tensile cracks to form a macro shear fault.

Scholz [1968] postulates a "critical density" of microcracks that must be reached before the fault can begin to form. Near the peak strength it was thought that the small flaws begin to interact to form a narrow zone of en echelon cracks which eventually becomes the shear fracture plane [*Horii and Nemat-Nasser*, 1985].

A different hypothesis is proposed by *Reches and Lockner* [1994]. Sophisticated experiments were conducted that control the rate of acoustic emission during loading, allowing for a very detailed examination of failure [*Lockner et al.*, 1991]. These experiments show that as a homogeneous rock (Westerly granite) is loaded to the peak stress, cracking is randomly located and fairly diffuse. However, as the peak stress is approached, a small process zone of cracks forms near the sample edge. It is postulated that at this point the tensile cracks interact, enhancing the dilation of one another such that more microcracks form in an unstable manner, producing an en echelon crack array. This process zone then propagates into the unfaulted sample and a macroshear fault follows behind in the brecciated zone by a mechanism of buckling or kinking of tiny rock columns [*Sammis and Ashby*, 1986].

Studies have also been conducted on the micromechanics of brittle failure in porous rocks, specifically sandstone [*Menendez et al.*, 1996; *Wong et al.*, 1997]. These studies show that in sandstones, shear localization usually does not develop until after the peak stress has been reached. Most of the cracking occurring before the peak stress appears to be intergranular (between grains). This is a departure from low-porosity crystalline rocks (granite) in which many of the cracks are intragranular [*Tapponnier and Brace*, 1976]. In sandstones it appears that most cracking occurs along grain boundaries, either by widening of preexisting microcracks or by shear rupturing of the cement at the grain contacts caused by rotation and slip of the grains. The high level of acoustic emissions (AE) recorded during dilation gives evidence that this second process is occurring.

Paper number 2000JB900085.
0148-0227/00/2000JB900085$09.00

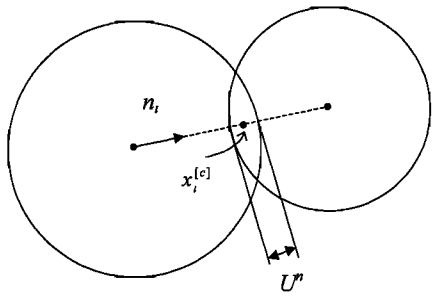

Figure 1. Ball-ball contact in PFC^{2D}. Symbols are explained in the text.

Using numerical models to further explain the observed cracking and failure in brittle rock is becoming more and more feasible as computer power increases. Statistical methods are often used in which an elastic rock is assigned some random crack population and failure on these cracks is observed as stress increases [e.g., *Blair and Cook*, 1998; *Salamon*, 1993; *Lockner and Madden*, 1991]. Boundary element methods have also been used to observe crack growth in polygonal grain assemblies [*Malan and Napier*, 1995]. These models have successfully reproduced some of the observed features of the fracturing process in rock, namely, the initial growth of tensile cracks that coalesce into inclined bands of localized shear strain. However, these models fail to consider energy (stress waves) released from the cracks and fractures. It is possible that these stress waves may effect rock fracture on all scales from microcrack formation to fault slip around mine workings [*Hildyard et al.*, 1995] to triggering of tectonic scale earthquakes [*Hill et al.*, 1993].

The purpose of this research is to create and examine the behavior of numerical models in which cracks and fractures can form spontaneously and release energy in the form of seismic waves. Itasca Consulting Group's Particle Flow Code (PFC) is a modeling package capable of doing this. PFC is a distinct element technique in which a rock is represented by an assembly of round particles and the equations of motion are solved using a time-stepping, explicit scheme [*Cundall and Strack*, 1979]. This scheme is based on a network of blocks (round particles) and springs where competent rocks can be modeled by bonding together the particles at points of contact. These rock models can then crack and fracture under stress as the bonds break. When a bond breaks, the stored strain energy at the contact is released in the form of seismic waves.

The distinct element method has been used successfully to examine several different geological applications. Shear band formation in granular material has been examined in depth [*Antonellini and Pollard*, 1995; *Cundall*, 1989; *Morgan and Boettcher*, 1999], earthquake faults with gouge have been simulated [*Mora and Place*, 1998], and *Donzé et al.* [1996] have used it to model an explosive source in a brittle rock mass. However, there is less published information on the use of distinct element codes to simulate failure of fully competent rocks under compression. *Potyondy and Cundall* [1998] use the PFC to examine cracking and breakout around tunnels in crystalline rocks. In the work presented here, similar techniques will be used to create models of three different rock types (two granites and a chalk) that will each be subjected to different compressive loading conditions. Cracking and the formation of fractures in the granite models will be examined in detail and compared to actual laboratory observations. In particular, the effect of dynamic waves on the failure process will be observed.

2. Theory

2.1. Bonded Particle Models

The PFC in two dimensions is a distinct element code that represents a rock mass as an assemblage of round disks confined by planar walls. The particles move independently of one another and interact only at contacts. They are assumed to be rigid (nondeformable), but deformation (or overlap) can occur at the contacts. Contacts are assumed to exist only at a point and not over some finite surface area as would be the case with fully deformable particles.

An example contact is shown in Figure 1. The contact point between the two particles ($x_i^{[C]}$) exists in a volume of overlap on a line joining the two particle centers. The normal force at the contact (ith component) is calculated by the force-displacement law:

$$F_i^n = K^n U^n n_i, \tag{1}$$

where K^n is the normal stiffness (force-displacement) at the contact, U^n is the normal displacement (overlap), and n_i is the ith component of the unit normal vector. Calculating the shear contact force is more complicated, as it has to be calculated in an incremental fashion. The change in shear force at a contact over one time step is

$$\Delta F_i^s = -k^s \Delta U_i^s, \tag{2}$$

where k^s is the shear stiffness that relates incremental displacement and force (compared to K^n that relates total displacement and force) and ΔU_i^s is change in the shear component of contact displacement. The shear contact force is then found by summing the old shear force at the start of the time step with the change in shear force over the time step:

$$F_i^s \leftarrow F_i^s + \Delta F_i^s. \tag{3}$$

The motion of a particle is then determined by the resultant force and moment vectors acting upon it using the law of motion. The equation for translational motion is simply

$$F_i = m\ddot{x}_i, \tag{4}$$

where F_i is the resultant force, m is the mass of the particle, and $\ddot{x}_i$ is the translational acceleration (this assumes no gravitational or other body forces). There is, of course, a similar equation for rotational motion. These law of motion equations are then integrated twice to obtain particle positions, which can then be used in the force-displacement calculations (1) and the calculation cycle starts again.

Equations are solved using a centered finite difference procedure involving a time step of Δt. The time step Δt is chosen to be so small that disturbance cannot propagate from any particle farther than its immediate neighbors. Therefore it is assumed that particle velocities and accelerations are constant within each time step. The forces acting on any particle are then determined exclusively by its interaction with the particles in which it is in contact. The calculation scheme is the same as that used in explicit finite difference methods for continuum analysis. This scheme is useful because of its ability to model dynamic problems accurately and efficiently; that is, it allows dynamic waves to propagate through the simulated rock in a realistic manner. For stability to be maintained, the time step

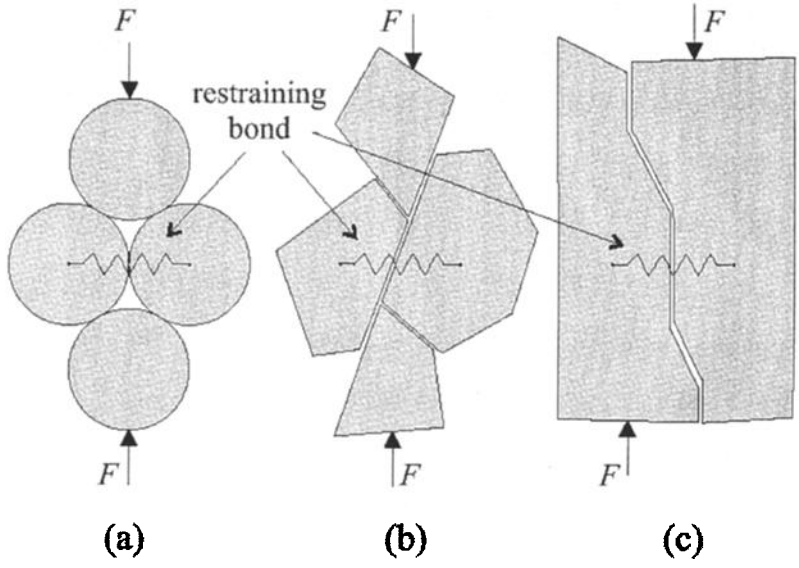

Figure 2. Physical mechanisms for axial cracking [from *Potyondy and Cundall*, 1999] (reproduced with permission from Itasca Consulting Group).

Δt must not exceed a critical time step that depends on the stiffnesses, densities, and geometry of the particles.

As well as deformation at the contacts, slip can occur between particles. The slip is defined by the friction coefficient at the contact μ. If there is no overlap between entities, then both the normal and shear force are set to zero. If the forces are greater than zero (i.e., there is overlap), then the contact is checked for slip by calculating the maximum allowable shear contact force:

$$F^s_{\max} = \mu |F^n_i|. \tag{5}$$

If $|F^s_i| > F^s_{\max}$, then slip is allowed to occur by setting the magnitude of F^s_i equal to $F^s_{\max}$.

A cohesive rock can be modeled (instead of just an assemblage of grains) by bonding together particles at contact points. When forces at any bond exceed the bond strength, the bond breaks. A contact bond can be visualized as a spot of glue of a vanishingly small size joining the two particles at the contact point. No slip is allowed while the bond exists; instead the magnitude of the shear force is limited by the shear contact bond strength. Note that the shear bond strength does not depend on the normal force at the contact. Contact bonds also bind the balls together and allow tensile forces to exist. The tensile normal force is calculated from (1) for $U^n < 0$, and the force drops to zero when the bond strength is exceeded and the bond breaks.

For the purpose of this research, each bond breakage is assumed to be a microcrack in the modeled rock. If a bond's shear strength is exceeded, then the crack will be called a shear crack; when a bond's normal strength is exceeded, a tensile crack is the result. The crack orientation is assumed to be perpendicular to the line joining parent particle centers. The bonded-particle approach is described in more detail by *Potyondy et al.* [1996].

2.2. Numerical Damping and Attenuation

In real rocks some energy is always attenuated by internal friction, scattering, etc., therefore it needed to be determined what level of numerical damping in PFC would approximate realistic levels of attenuation in the models. A common measure of attenuation or energy loss in real rocks is the seismic quality factor Q. Q is defined as 2π times the ratio of stored energy to dissipated energy in one wavelength:

$$Q = 2\pi(W/\Delta W), \tag{6}$$

where W is energy.

Therefore a wave passing through a rock with high Q will experience little attenuation. In PFC^{2D}, frequency-independent damping is applied by specifying a damping coefficient α. The damping force applied to each particle is then given by

$$F^d = -\alpha |F| \text{ sign } (V), \tag{7}$$

where $|F|$ is the magnitude of the unbalanced force on the particle and sign (V) is the sign (positive or negative) of the particle velocity.

For a single degree of freedom system, α can be expressed in terms of energy loss in one cycle by

$$4\alpha = \Delta W/W. \tag{8}$$

Combining (6) and (8) therefore yields

$$Q = \pi/2\alpha. \tag{9}$$

Equation (9) can be used to estimate the numerical damping required in a PFC model to reproduce the required level of wave attenuation.

3. Justification for Use

The mechanical behavior of rock under compression is known to be governed by the formation, growth, and interaction of microcracks. These cracks are thought to be predominantly tensile and oriented approximately parallel to the maximum compressive stress direction. The micromechanics of how these cracks form is not fully understood, although many possible mechanisms have been proposed (e.g., pore crushing, sliding along preexisting planes of weakness, elastic mismatch between grains). In PFC the mechanism by which tensile cracks form is the wedging apart of two round particles by an axial load (see Figure 2). Similar mechanisms may occur in

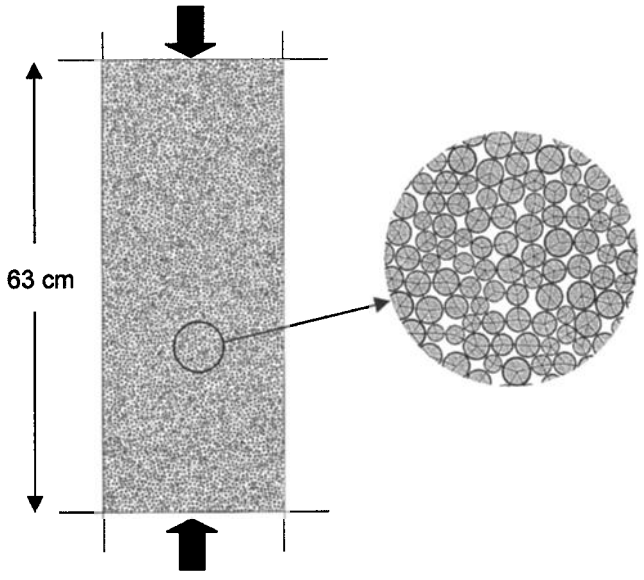

Figure 3. PFC^{2D} model of Lac du Bonnet granite. Thick arrows show the direction of applied stress. Thin lines show the location of bonds connecting the particles.

actual rocks with angular grains (see Figure 2) suggesting that PFC may be used to simulate the mechanical behavior of crystalline, as well as sedimentary rocks. The method of tensile crack formation in PFC is obviously a simplification of what occurs in reality; however, *Kemeny* [1991] shows that virtually all tensile crack mechanisms can be approximated by a pair of point loads acting at the center of the crack. It is proposed that the mechanism of tensile crack formation in PFC provides an adequate representation of this process.

Furthermore, it is thought that for localization and failure in real rocks to occur, there must be interaction between microcracks [*Okui and Horii*, 1995]. In PFC this interaction occurs naturally because localized bond breakages induce global stress redistribution.

Of course, this modeling approach still represents a significant simplification of the processes that occur in reality. In particular, the fractal nature of fracture networks in rocks is not reproduced since a fairly uniform array of crack sites is being used. However, three examples follow that show that the macromechanical behavior of some rock types can be well simulated by using a simplified micromechanical structure as is used in PFC. These analyses are presented here to give confidence that this type of modeling can successfully reproduce rock behavior under compression and can therefore be used in the more detailed studies of cracking and failure that follow.

All of the models presented in this section (section 3) are run with high levels of attenuation to artificially damp dynamic waves so as to mimic quasi-static calculations. Models with realistic, rock-like levels of attenuation are presented in sections 4 and 5.

3.1. Lac du Bonnet Granite

The mechanical behavior of Lac du Bonnet granite has been studied extensively as part of a feasibility study into the concept of underground nuclear waste disposal [see *Martin*, 1993]. In addition to laboratory and field tests on Lac du Bonnet granite, extensive modeling of this rock type using PFC has been performed [see *Potyondy et al.*, 1996].

3.1.1. Choice of microparameters. In this study, a 252 × 630 mm model core sample of Lac du Bonnet granite was created using approximately 6500 particles ranging in diameter from 4 to 6 mm (see Figure 3). This sample size is the standard used in many mechanical tests conducted by Atomic Energy of Canada Limited in their studies of this rock type. The particles in the model are approximately equal to the size of actual mineral grains in Lac du Bonnet granite [*Kelly et al.*, 1993].

The Young's modulus of Lac du Bonnet granite is approximately E = 65 GPa, and the unconfined compressive strength is approximately σ_c = 213 MPa [*Read and Martin*, 1992]. The microparameters used to reproduce this behavior with a PFC model are shown in Table 1. Note that the values assigned to these microparameters do not correspond directly to the elastic properties of the whole sample because of the random, irregular particle packings. For a given rock type the required microparameters are determined indirectly by assigning values and comparing the response of the synthetic material to the relevant measured responses of the intended physical material. The microparameters are then adjusted so that the desired behavior is more accurately reproduced.

In general, the stiffnesses assigned to the particles influence the overall stiffness of the sample, and the ratio of normal to shear stiffness influences the Poisson's ratio. The bond strengths determine the strength of the simulated material, and the standard deviation in bond strengths (the strengths are assigned a Gaussian distribution about the mean) influences the nature of failure. A high standard deviation produces a gradual failure, while a narrow range in bond strengths produces rapid failure when the peak stress is approached. The ratio of normal bond strength to shear bond strength influences the nature of sample failure and the abundance of tensile cracks versus shear cracks.

The packing of the particles has a minor influence on both the stiffness and strength of the model (±5%). The particle and sample size does not generally influence the rock behavior

Table 1. Microparameters Used in PFC Modeling

Microparameter	Description	Lac du Bonnet Granite	Westerly Granite	Ekofisk Chalk
E_c, GPa	Young's modulus at contact	100	100	6
K_n/k_s	ratio of particle normal to shear stiffness	2	2	4
μ	particle friction coefficient	0.7	0.7	0.3
σ_c (mean), MPa	average normal bond strength	162	300	100
σ_c (s.d.), MPa	standard deviation of distribution of normal bond strengths	44	80	30
τ_c (mean), MPa	average shear bond strength	243	450	100
τ_c (s.d.), MPa	standard deviation of distribution of shear bond strengths	66	120	30

because the appropriate scaling relationships are accounted for in the code. The particle stiffness (K'' in equation (1)) does not need to vary with particle size to maintain a constant overall modulus; however, the contact bond strength must vary inversely with the particle radii to maintain a constant strength.

The scaling relationships can be explained by thinking of two bonded particles (disks in two dimensions). The maximum normal stress at the contact will be the bond strength (in units of force) divided by the area. If we assume the area is the cross-sectional area of the disk ($2Rt$, where R is the radius and t is the thickness), then

$$\sigma_c = S_n/2Rt, \tag{10}$$

where S_n is the bond normal strength. The contact Young's modulus can be calculated by dividing incremental stress by incremental strain so that

$$E_c = \frac{\Delta\sigma}{\Delta\varepsilon} = \frac{F_n/A}{\Delta\varepsilon} = \frac{k_n \Delta R/2Rt}{\Delta R/R} = \frac{k_n}{2t}, \tag{11}$$

where k_n is the incremental particle normal stiffness. Equations (10) and (11) are derived for only a single contact but they illustrate that the overall modulus of a two-dimensional (2-D) assembly is proportional to particle stiffness but independent of radius (equation (11)), while the overall strength depends on the bond strength and particle radius (equation (10)). The values of contact strength and stiffness derived in (10) and (11) correspond to the microparameters shown in Table 1 (a thickness of $t = 1$ was used in all models). Note that the contact microparameters will be different from the macrostrength and stiffness of the overall assembly because of the random packing of the particles.

3.1.2. Testing. The Lac du Bonnet granite sample was uniaxially loaded by deleting the sidewalls and moving the top and bottom walls (platens) together at a constant velocity of 0.2 m/s (note that the P wave velocity in this rock type is ~6000 m/s). The loading velocity has little effect on the mechanical behavior of the modeled sample as long as it is slow enough to ensure that no transient waves are being produced. Note that this not true if creep/stress corrosion is accounted for in the model. A sophisticated algorithm that considers stress corrosion and relates bond strength to duration of loading is described by *Potyondy and Cundall* [1998], but for simplicity, this will not be used here.

The stress-strain behavior of the model compared to the stress-strain behavior observed in an actual unconfined laboratory compression test is shown in Figure 4. It can be seen that the shapes of the curves are similar and that the strength and stiffness of the rock are approximately reproduced by the model. No attempt was made to reproduce exactly the strength and stiffness of the rock due to the random nature of both the PFC model and actual rock samples. Also, no attempt was made to reproduce the Poisson's ratio of the granite because the ratio of lateral strain to axial strain in PFC^{2D} is not strictly comparable to Poisson's ratio of a real three-dimensional material. Full three-dimensional models would be required to obtain directly comparable Poisson's ratios.

The most obvious difference between the model and rock response is the lack of initial curvature observed during the laboratory tests at low stress levels. This curvature is absent from the model response because there are no preexisting cracks in the model. Owing to the explosive nature of the sample failure in the laboratory tests, no postpeak information was recorded, so comparisons cannot be made with the model results over this part of the stress-strain curve. However, the gradual strength reduction observed in the model curve of Figure 4 after the peak stress suggests that the model is not experiencing explosive sample failure. It will be shown in section 4 that when the model is run dynamically with realistic, low levels of attenuation, a more dramatic strength reduction after the peak stress is observed.

An extensive study of the effects of all of the microparameters and the effects of different levels of confinement on the sample behavior has been performed [*Potyondy and Cundall*, 1999] but will not be reproduced here because of space limitations. The main purpose of this paper is to examine the cracking and failure patterns in the modeled Lac du Bonnet granite and the effect of dynamic waves on these patterns. These results will be presented in section 4.

3.2. Westerly Granite

A similar model was created to simulate a core sample of Westerly granite being subjected to axial compression with a confining stress of 50 MPa. A model of a core sample measuring 190.5 mm by 76.2 mm was created to simulate experiments done by *Lockner et al.* [1991]. Owing to the small grain size of this rock type (0.1 mm), it was not feasible to produce a model in which every particle represented a single mineral grain. Therefore each particle is assumed to be a small, representative volume of say 5–10 mineral grains. This led to a model composed of 8775 particles with an average particle radius of 0.65 mm. It was found that even with this simplification, the major behavioral properties of Westerly granite were reproduced. The microparameters used in this model are shown in Table 1. It can be seen that the bond strengths are higher than those for Lac du Bonnet granite to account for the increased strength of Westerly granite.

Axial load was applied to the model such that an approximately constant acoustic emission rate was maintained. This was done to reproduce the experiments conducted by *Lockner et al.* [1991] where they wished to slow down the fracture process to allow for detailed examination of fracture propagation. This type of loading was achieved in the model by applying a servomechanism to the top and bottom walls so that the wall velocities were constantly updated to maintain the desired cracking rate. Note that both in the laboratory test and the model the loading direction had to be reversed during fracture growth.

A comparison of the stress-strain behavior produced by the model compared to the actual behavior recorded during a laboratory test on Westerly granite is shown in Figure 5. As with the Lac du Bonnet granite model, the model and the actual sample show approximately the same stiffness and strength. Unlike the Lac du Bonnet granite model, the different boundary conditions applied to the Westerly granite model cause rapid strain weakening in the postpeak region. This agrees with what is observed in the laboratory study. Notice in the plot of the modeled stresses that there are small episodic stress drops and recoveries as the peak stress is approached. These correspond to small bursts of AE activity and rapid unloading of the system. The same behavior was noticed in the laboratory experiments [see *Lockner et al.*, 1992]; however, the jumps were much smaller; presumably because the AE in the lab experiment were much smaller and more plentiful and therefore each AE had less impact on the system.

The cumulative number of cracks recorded in the model is

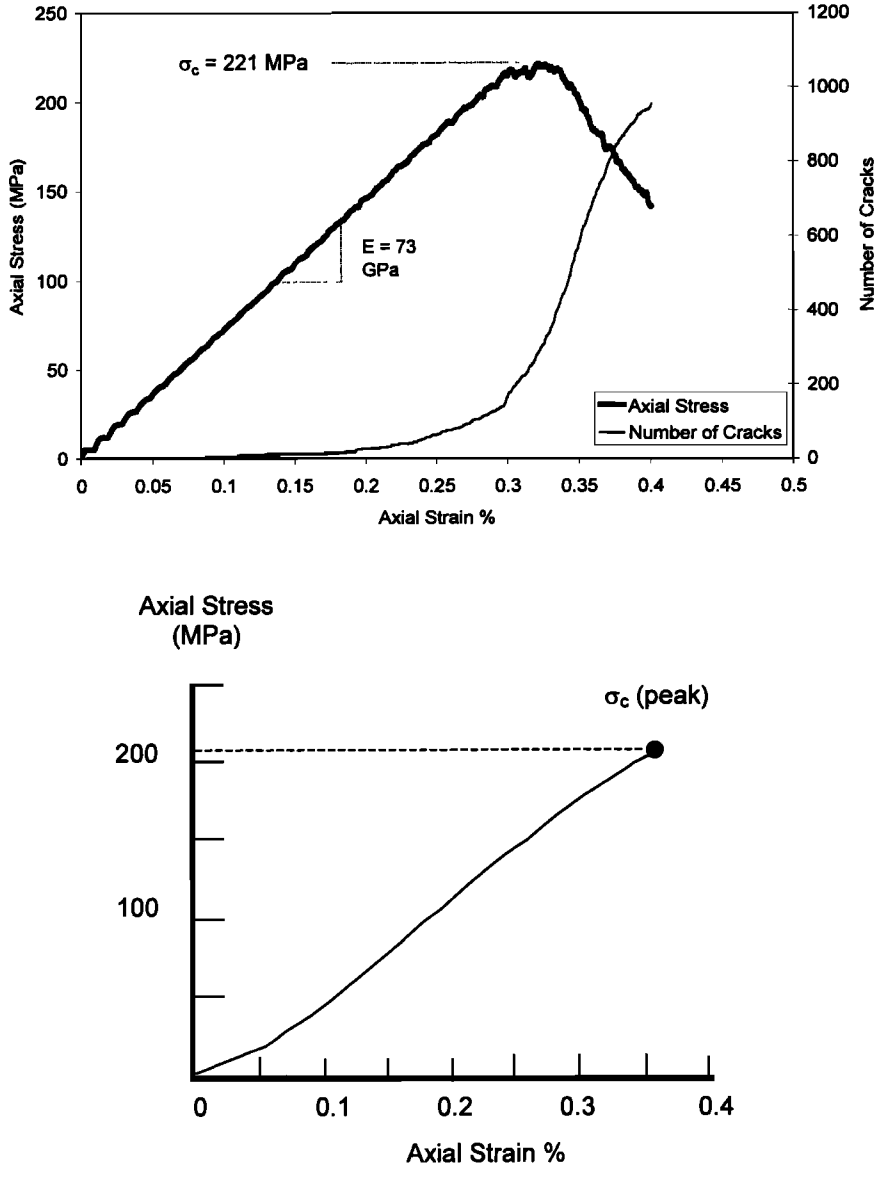

Figure 4. (top) The stress-strain response and number of cracks occurring during unconfined loading of the Lac du Bonnet granite model compared to (bottom) a similar laboratory test [from *Martin*, 1993]. The model is run with high numerical damping (α = 0.7).

plotted versus time in the inset in Figure 5a to show the success of the servomechanism at maintaining a constant acoustic emission rate. Figure 5 shows that the line is generally straight with only a few small deviations where small crack clusters formed before the loading walls could compensate.

3.3. Ekofisk Chalk

The mechanical behavior of Ekofisk chalk has been studied extensively to try to understand the compaction of hydrocarbon reservoirs in the North Sea [e.g., *Leddra et al.*, 1990]. This rock type is obviously much softer and much more porous than granite (porosities can reach 50%). However, by adjusting the particle geometries and the microparameters the mechanical behavior of this chalk can be well reproduced by PFC models.

A model of a 25 × 50 cm core sample was created using 9000 particles ranging in size from 0.5 to 3.25 mm. Note that it would be infeasible to model the actual grains of the chalk, so each particle is assumed to represent a small representative volume. The grains were initially densely packed, as with the granite model described above. Three models with porosities of 28%, 38%, and 48% were then created by sequentially deleting the largest particles until the desired porosity was attained. Note that the actual porosities of the PFC models are not the same as the porosities of the corresponding chalk samples. This is because for a given distribution of disks in two dimensions the area-based porosity will be significantly less than the volume-based porosity for an assembly of spheres in three dimensions (e.g., *Deresiewicz* [1958] shows that the closest regular packing of uniform spheres in three dimensions has a porosity of 0.2595, while the closest regular packing of uniform disks in two dimensions has a porosity of 0.0931). For the particle assembly used here, the ratio of 2-D to 3-D porosity that produced the best results was found experimentally to be ~0.8. Therefore the samples with 28%, 38%, and 48% volumetric porosities were modeled by 2-D samples with 22%,

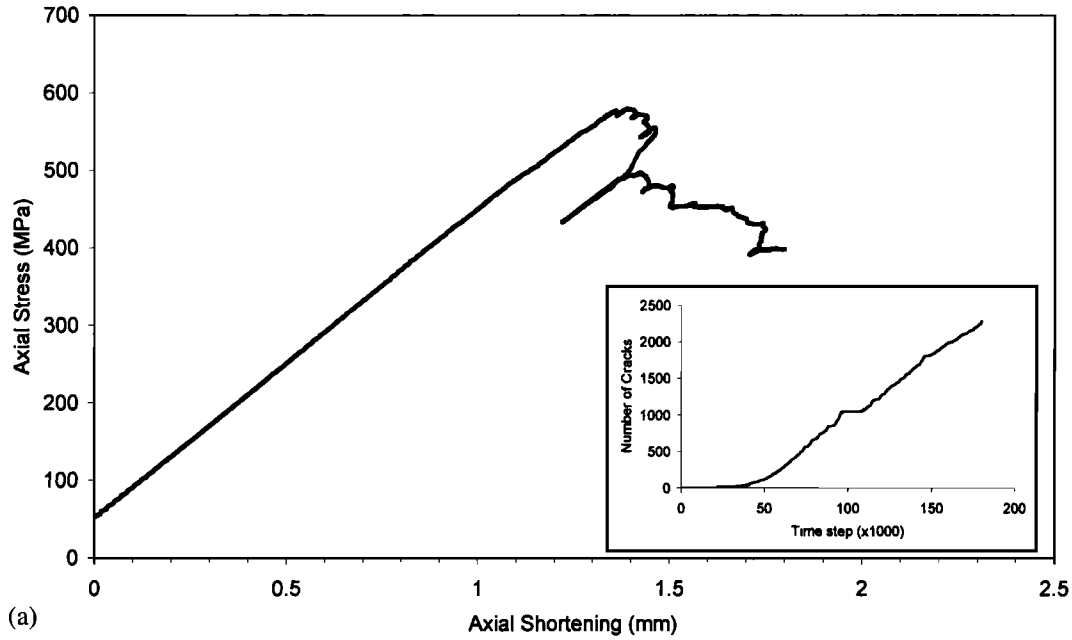

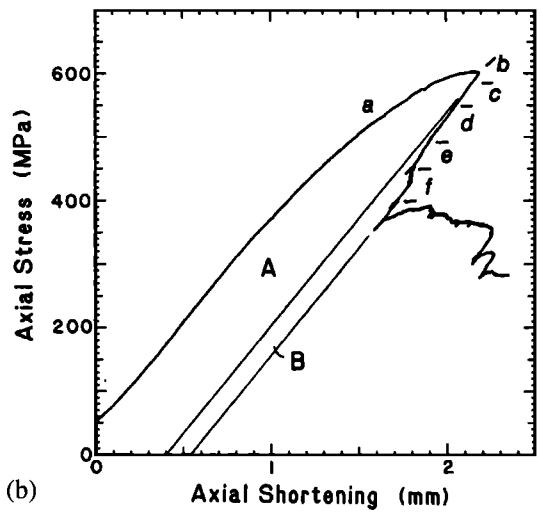

Figure 5. Stress-strain response of PFC model of (a) Westerly granite loaded with 50 MPa confining stress compared to (b) a similar laboratory test [from *Lockner et al.*, 1991] (copyright permission granted by *Nature*). Letters in Figure 5b correspond to plots shown in Figure 14. The inset in Figure 5a shows the cumulative number of cracks plotted against the model time step. The model is run with high numerical damping (α = 0.7).

30%, and 38% area porosities. The 38/30% porosity model is shown in Figure 6.

The particle stiffnesses were chosen so that the initial elastic stiffnesses of the models (before any bond breakages) corresponded with the initial elastic stiffnesses observed in laboratory tests. The bond strengths were then chosen so that cracking and pore collapse would start at ~2–3% strain as observed in the laboratory tests. Note that all three models (28%, 38%, and 48% porosity) were assigned the same values for the microparameters (see Table 1). Only the porosities varied between the three models. The modeled samples were then loaded axially with no lateral strain permitted to simulate the conditions of the laboratory tests.

The stress-strain behavior of the three models plotted with the laboratory data is shown in Figure 7. It is clear that the models simulate very well the laboratory behavior for all three different porosities, even though all microparameters are the same. It is encouraging that no complicated constitutive laws are required to reproduce the stress-strain behavior as would be the case in most continuum models. This gives confidence that the micromechanical approach used by PFC is capable of reproducing a large range of rock mechanical behavior.

4. Evolution of Shear Fracture in Lac du Bonnet Granite Model

The model of Lac du Bonnet granite described in section 3.1 was used to examine in detail the cracking and failure that

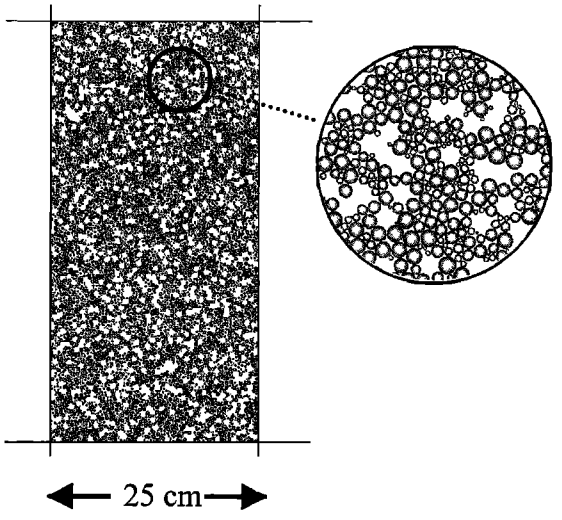

Figure 6. PFC model of a 38% porosity sample of Ekofisk chalk.

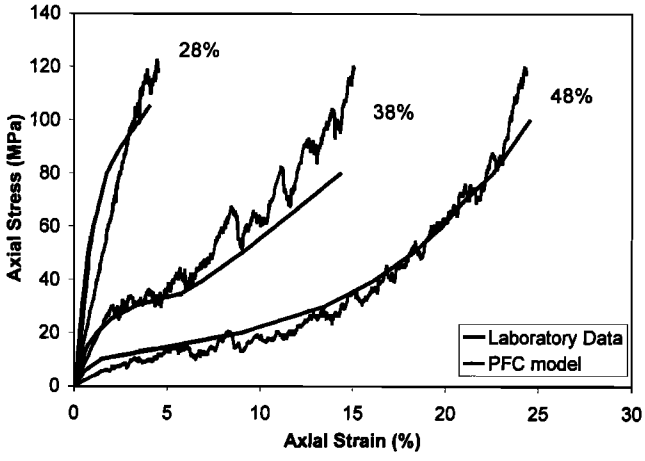

Figure 7. The stress-strain behavior of three chalk models of different porosities subjected to axial loading, with no lateral strain permitted, compared with recorded laboratory behavior (laboratory data from *Leddra et al.* [1990]).

occurs during loading. The model was rerun with all of the microparameters the same except the numerical damping. In the above models, a high level of numerical damping was applied. This means that energy was extracted from the system each calculation step to speed the models to convergence. The purpose of this research, however, is to examine the evolution of cracking during loading and how the energy released from each crack affects the rock behavior. Therefore much lower levels of damping were required to allow energy to be emitted from each crack in the form of seismic waves.

4.1. Effect of Damping on Cracking and Strength

The stress-strain behavior shown in Figure 4 resulted from running the granite model with a damping coefficient, α of 0.7, which corresponds to a quality factor, Q of 2.2 by (9). This is not a totally realistic representation of granite as it is known that most granites are quite competent and that waves are not severely attenuated. To try and simulate more realistic conditions, the model was run with much less damping so that the waves were free to propagate through the rock sample. The quality factor of Lac du Bonnet Granite in situ is about 220 [*Feustel*, 1995]; however, for a core sample full of stress relief fractures it is likely that Q will be significantly lower. A value of $\alpha = 0.015$ was therefore chosen for the model which yields a quality factor Q of 100.

The results obtained when this low value of damping was applied are shown in Figure 8. It is clear that the strength of this modeled sample is significantly lower than the strength of the model run with high damping (by ~15%). Also the failure seems to be more severe, with much more rapid crack growth when failure is approached. The line showing the cumulative number of cracks increases in discrete jumps in Figure 8, whereas the cracking appears to form more uniformly in the highly damped model (Figure 4). This indicates that cracking may be occurring in clusters in the dynamically run model. The reasons for these differences will be explained in sections 4.2 and 4.3.

4.2. Microcracking

The granite model was axially loaded again but with a 20 MPa confining pressure applied to encourage the growth of a shear macrofracture. Bond breakages (cracks) were monitored throughout the test. The numerical damping was set to $\alpha = 0.015$ (as in section 4.1) meaning that the quality factor of the model was $Q = 100$.

Figure 9 shows the location, orientation, and nature of cracking (tensile or shear) that occurred over the whole loading test. It appears that most of the cracks are tensile and subvertical, oriented approximately parallel to the loading direction. This agrees with laboratory studies on axially loaded cylinders that show predominantly tensile cracking oriented parallel to σ_1. Figure 9 also shows that many of the microcracks formed along a macrofracture at ~40° to σ_1. This is again consistent with laboratory observations that generally show failure of samples along inclined shear fractures. The angle of the shear fracture that forms in actual rocks under compression depends on the level of confinement and the internal friction of the rock. A comprehensive study on how the angle of fracture in PFC models depends on confinement and friction angle, as well as particle packing geometries has not yet been performed.

To examine the evolution of the shear fracture in more detail, the cracks occurring before and after the peak stress are plotted in Plate 1, where the cracks are also colored according to time. Two important observations can be made from this plot. First, there is only sparse cracking before the peak stress, and the cracks are more or less randomly located. After the peak stress, however, there is clear localization of cracking along the macro shear zone. The second thing to observe is the timing of the cracking after the peak stress. The cracks appear to start at the right edge of the sample forming an inclined "process zone." A second zone of cracking then occurs in the top left corner, and these two clusters are joined by a third zone of cracking in the middle. Plate 1 shows how the cracks tend to form in large clusters rather than uniformly along the fault zone.

Compare this behavior with that of the same model run with high numerical damping ($\alpha = 0.7$). Plate 2 shows the cracks occurring in the model run with high damping before and after the peak strength. Many more cracks occur before the peak stress in this model, and many of these cracks are aligned along narrow, inclined zones. The cracks occurring after peak stress

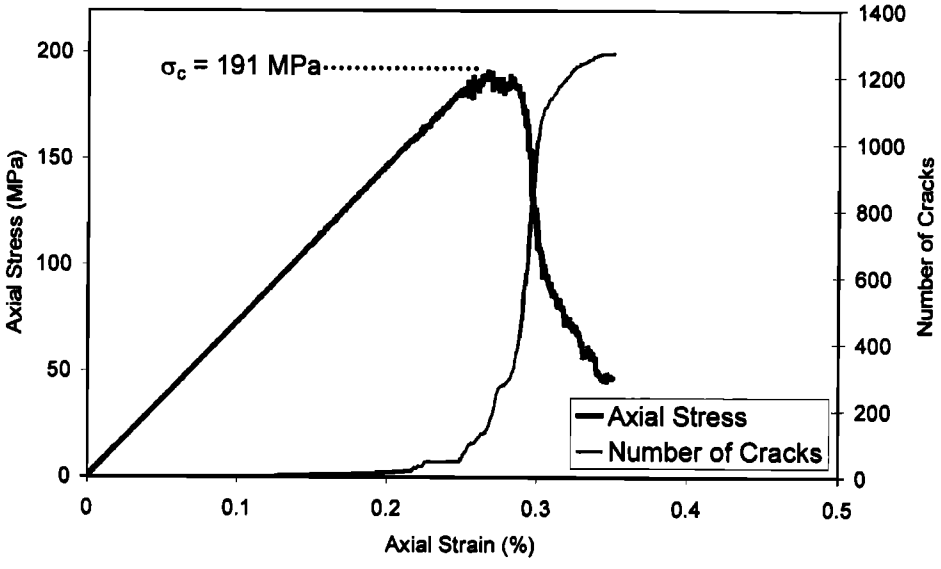

Figure 8. Stress-strain response of an unconfined loading test on the Lac du Bonnet granite model with a low damping of $\alpha = 0.015$.

appear to show no pattern with respect to their time of formation, i.e., cracks seem to be forming at all locations along the shear zone simultaneously. There are many small clusters of cracks along the fault zone, but the clustering is not nearly as pronounced as in the dynamically run model. The reasons for this will be explained in section 4.3.

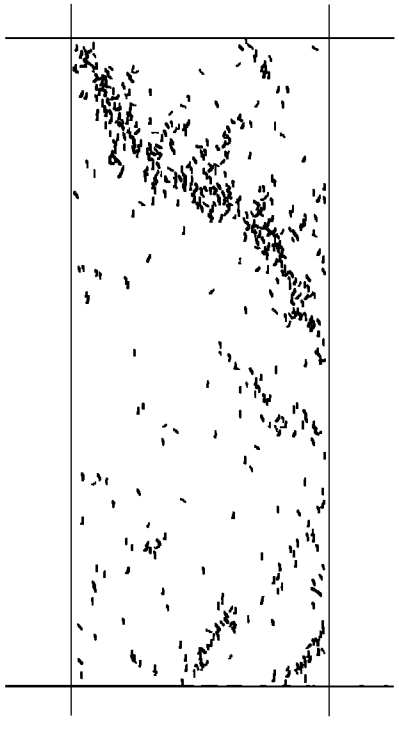

Figure 9. The location and orientation of all cracks occurring during loading of the Lac du Bonnet granite model with 20 MPa confining pressure. Dark lines represent tensile cracks, and light lines indicate shear cracks.

4.3. Crack Cluster Formation

When a tensile crack forms in PFC, a permanent zone of increased tension forms above and below the crack due to the shifting of particle positions. Previous studies have shown that when models are run dynamically, a larger and more intense transient zone of increased tension also forms due to the passing wave [*Hazzard*, 1998]. The question that needs to be answered is whether or not the waves emitted from the cracks are capable of instigating further cracking nearby, over and above the cracking that would be caused by static stress changes. If so this would help explain why the dynamically run model was weaker than the model run with high damping and also why larger crack clusters appear to form in the dynamically run model.

To examine this, the tensile forces at contacts around cracks were examined as stress waves passed by. These forces were then compared to the tensile strengths of the bonds to see if the effect of the passing waves would be sufficient to cause bond breakage. A typical plot is shown in Figure 10. It is obvious in Figure 10 that the passing wave from the nearby bond breakage would cause the bond to break. The passing wave creates a tension peak, whereas the long-term, "static" increase in tension at this site (assumed to be the average force at the contact after the first peak) would be insufficient to break the bond. Note that the stress change due to a passing wave will only cause a bond to fail if it is close to failure already. That is why crack clusters form near the peak stress but not before.

To examine this effect further, the initiation of localisation in the granite model was examined in detail. Figure 11 shows the velocities of the particles at the right edge of the sample where the formation of the shear macrofracture starts. The particle velocities (magnitudes) are shown at different times from the start of localization (the peak stress) along with the locations of newly formed cracks. It appears likely from Figure 11 that the waves emitted from each crack are causing the formation of more cracks nearby. If full damping is applied

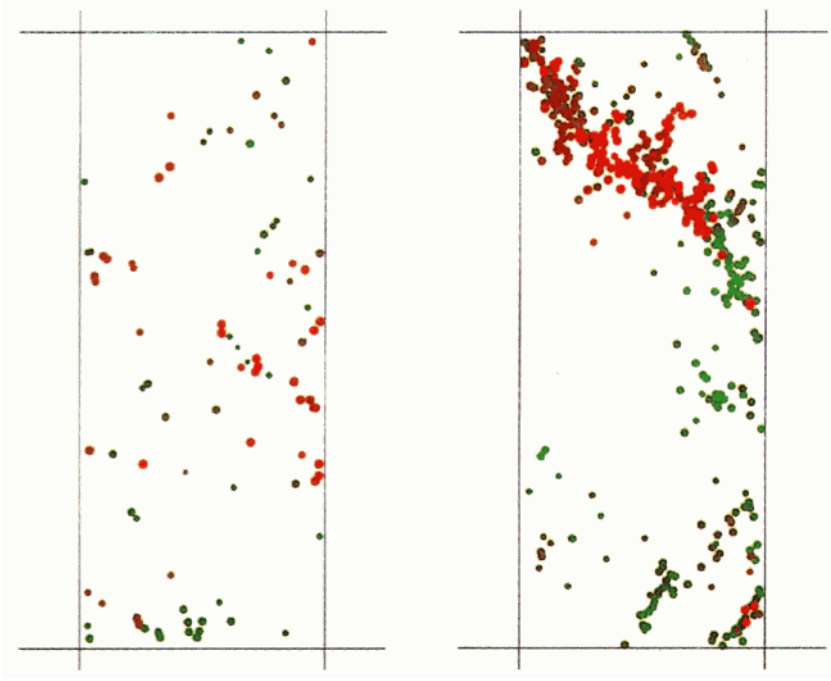

Plate 1. Cracks forming in the Lac du Bonnet granite model (left) before the peak stress and (right) after the peak stress in the dynamically run model. The color of the circle indicates the relative time that the crack occurred in each frame: green is early and red is late.

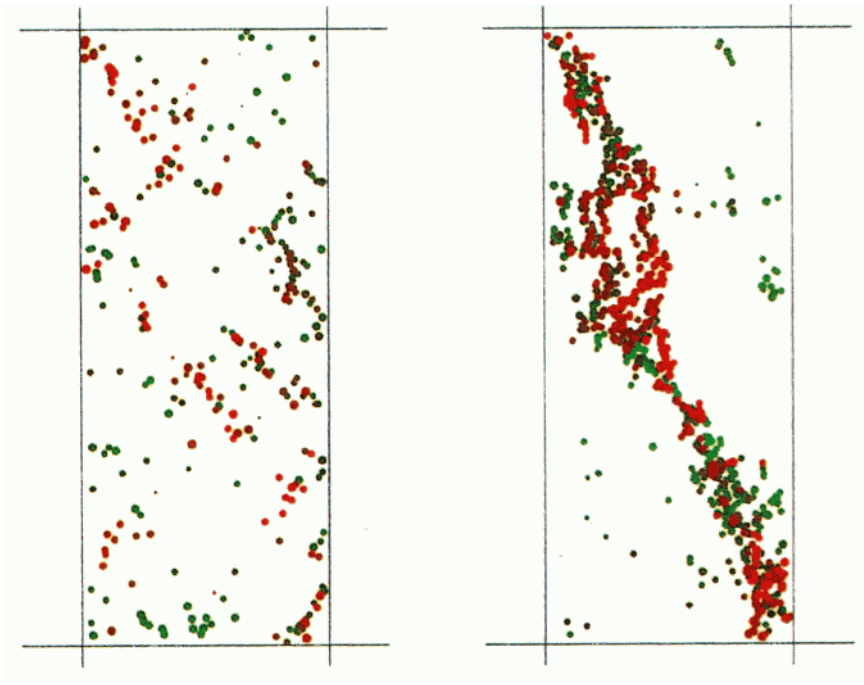

Plate 2. Cracks forming in the Lac du Bonnet granite model (left) before the peak stress and (right) after the peak stress in the highly damped model. The color of the circle indicates the relative time that the crack occurred in each frame: green is early and red is late.

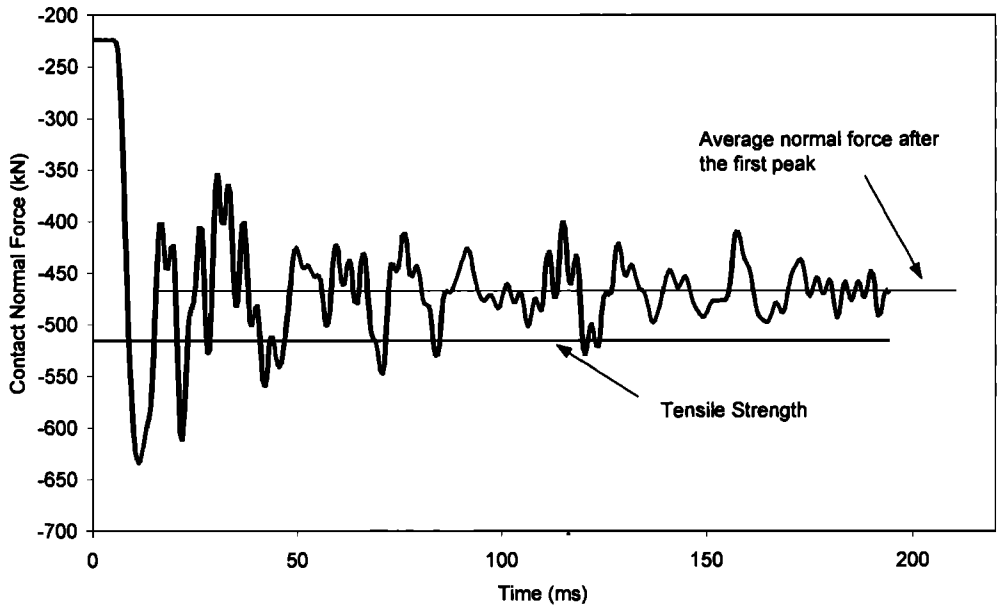

Figure 10. The normal force at a contact after a nearby bond breakage. Tensile forces are negative. The tensile strength of the bond is shown by the straight thick line and the average force at the contact after the first peak is shown by the straight thin line.

over the same time period, then fewer cracks form, and failure in the sample does not commence.

Even though the static stress change around cracks may induce more cracks to form nearby, the dynamic effect seems to be significantly greater. In the highly damped model the static change in stress around a crack is small, and therefore many contacts need to be close to failure before cracks can interact to cause sample failure. However, in the dynamic model, passing waves emitted by cracks cause larger stress changes that induce more cracks, eventually leading to earlier sample failure. This goes some way to explaining why the strength of the dynamically run sample is less then the strength of the sample in the high-damping test. This dynamic effect also explains why larger crack clusters tend to form in the dynamic model than in the highly damped model.

5. Evolution of Shear Fracture in Westerly Granite

The model of Westerly granite described in section 3.2 was rerun with low damping (α = 0.015). Most of the traits exhibited by the dynamically run Lac du Bonnet granite model are also observed in this Westerly granite model. The peak strength decreased by ~10% when the Westerly granite model was run dynamically (compare Figure 12 with Figure 5). Also the cracking occurs in discrete jumps in the dynamically run model as with the Lac du Bonnet granite model. The inset in Figure 12 shows that the cracks form in small bursts and the servomechanism that controls the loading is unable to back off fast enough to prevent these clusters from forming. Even if the rate of axial stress adjustment is increased fourfold, the same patterns are observed. This indicates that clusters of cracks are forming independently of the loading, lending weight to the idea that the cracks within a cluster are interdependent and are not directly induced by the loading stresses. Also, the increased size and number of the clusters in the dynamic simulation compared with the static model indicate that the dynamic effect is more significant than the static.

The cracking occurring during this test is shown in five time frames in Figure 13. The locations of AE recorded by *Lockner et al.* [1991] in an actual laboratory experiment on Westerly granite are also shown here for comparison (Figure 14). There are some similarities between these two plots. Before the peak stress (Figures 13a and 14a) the cracking is diffuse and scattered throughout the sample. In Figures 13b–13e and 14b–14e the cracks generally cluster along a narrow inclined zone of localization (fracture plane). Also, the cracks in the model appear to propagate outward from a definite starting point as in the laboratory study.

One difference is that areas along the fault that have already experienced cracking in the model do not show more cracking in subsequent frames, as in the laboratory test. This is because bonds do not reform in PFC, and once they are broken, no cracking will be recorded at the contact, even if the contact is slipping. Another difference is the small cluster of cracks that appears close to the bottom wall of the model. These cracks may have been caused by the rapid wall movement required to maintain the constant cracking rate. More investigation is needed into the source of these cracks.

6. Discussion and Conclusions

PFC models of rock appear to be able to reproduce many of the behavioral characteristics observed in real rock specimens, for example, stress-strain response and cracking and failure patterns. This is due to the micromechanical nature of the code and the ability to consider tensile crack formation in a compressive stress field. This is generally not possible with continuum models, and therefore complicated constitutive formulations are often assigned to reproduce observed rock behavior. With PFC some of the dominant processes are reproduced on the micromechanical level, and an opportunity therefore exists

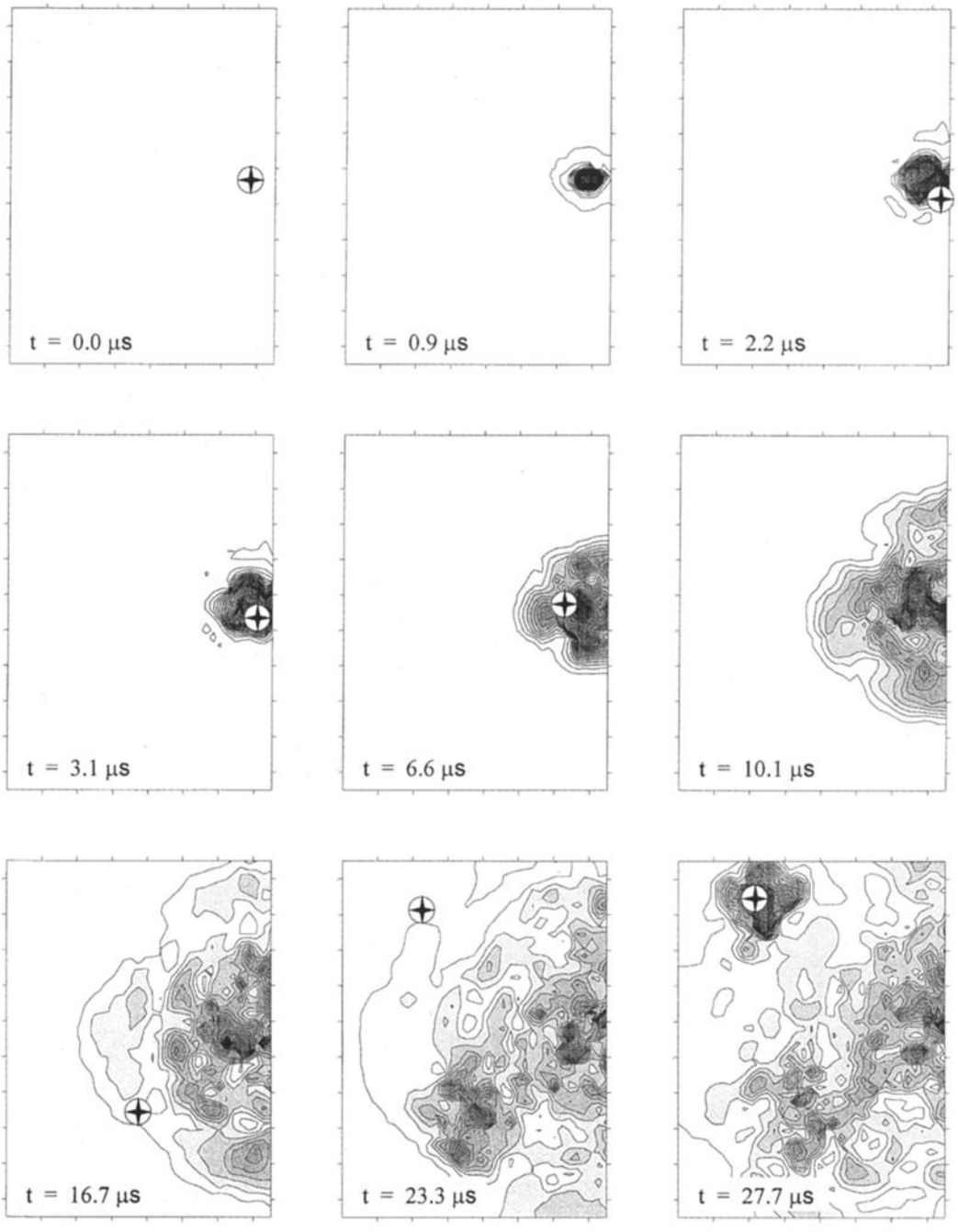

Figure 11. A closeup of the right edge of the Lac du Bonnet granite model (0.2 × 0.15 m) showing particle velocities and crack formation from the start of localization (peak stress). The contour interval is 0.2 m/s. New cracks are shown as four-pointed stars.

to investigate some of the micromechanical processes that may be occurring in rock that cause the observed macromechanical behavior.

This paper outlines how the mechanical behavior of different rock types can be reproduced by considering the micromechanical structure of the rocks. Stress-strain behavior of granites and chalk models corresponded well with behavior observed in laboratory tests. Cracking patterns in the granite models were also similar to those observed in laboratory tests, namely, that cracks were predominantly tensile and oriented parallel to σ_1 and that failure of the sample resulted from localization of this cracking along inclined shear bands.

It was shown that the energy released by cracks on the microscale may have a significant influence on the rock behavior. In the granite models presented in sections 3 and 4, the waves emanating from the cracks were capable of inducing more cracks if nearby bonds were close to failure. This lead to the formation of large crack clusters as the peak stress was approached and an eventual chain reaction of cracking causing sample failure. In models run with high levels of damping, the static stress changes around cracks were smaller in magnitude and extent and therefore did not induce large clusters to form. It was shown that the effect of the dynamically induced cracking was to decrease the overall strength of the sample by up to 15%.

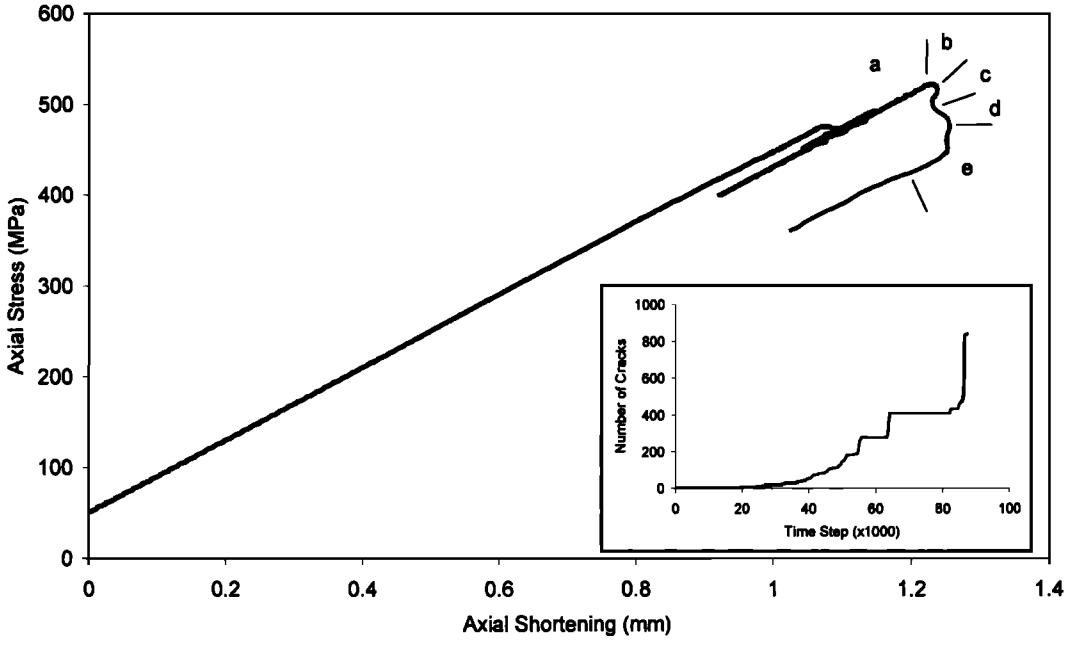

Figure 12. Stress-strain behavior of dynamically run Westerly granite model ($\alpha = 0.015$). Letters correspond to plots shown in Figure 13. Inset shows the cumulative number of cracks plotted against model time step.

The dynamic waves produced by the cracks also influenced the nature of the failure. It was shown that when the peak stress was approached, intense microcracking started and a macrofracture propagated into a basically unfractured sample by means of joining of distinct crack clusters. The sample eventually failed when these crack clusters grew to bisect the sample. This behavior is similar to that observed in actual laboratory tests, except that in the laboratory, only one crack cluster forms that propagates across the entire sample.

If the waves emitted from the cracks are suppressed then different failure patterns result. Crack clusters still form, but they are much smaller. The shear localization appears to forms more by a coalescence of small clusters rather than a propagation. This is in contrast to laboratory observations and may indicate that the effect of dynamic waves may need to be considered in future models to accurately reproduce actual rock behavior.

The instigating of new cracks by the stress waves of previous cracks clearly happens in PFC^{2D} but does this happen in reality? If so, this could have important implications for larger-scale seismology problems where waves emitted from earthquakes may trigger even distant earthquakes [*Hill et al.*, 1993]. Perhaps more importantly, the dynamic interaction of small events in the near field (as shown here) may be determining the size of the mainshock and the mechanics of the source [*Harris and Day*, 1993].

Many possibilities exist for future study using this modeling approach. The micromechanics of tensile crack formation in PFC are probably more akin to what occurs in a well-sorted sandstone, rather than a crystalline granite. Therefore the

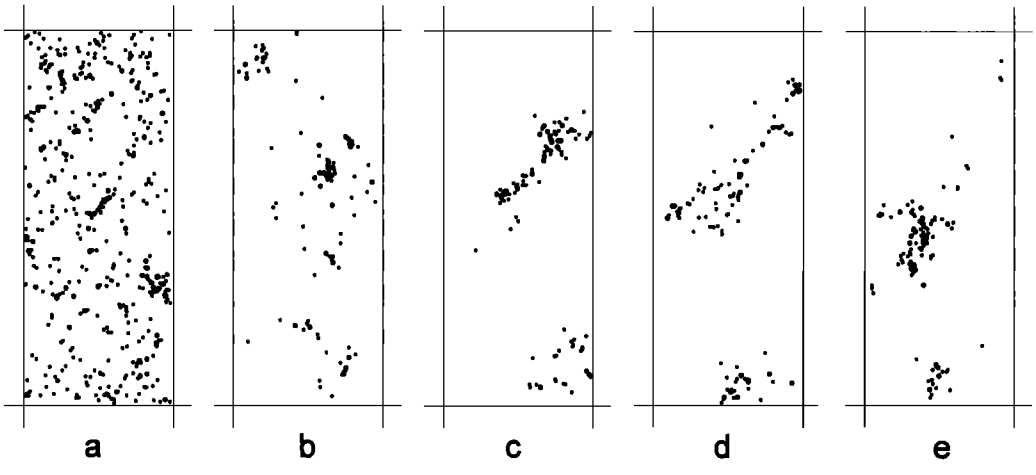

Figure 13. Cracking occurring during five successive stress intervals during failure of the Westerly granite model. The intervals are shown in Figure 12.

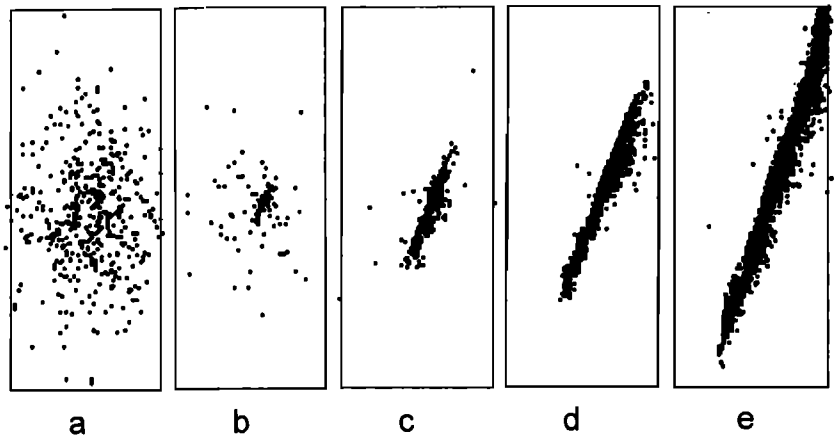

Figure 14. Acoustic emissions for five intervals recorded in an actual laboratory test on Westerly granite [from *Lockner et al.*, 1991] (copyright permission granted by *Nature*). Intervals are shown in Figure 5.

compressive loading tests on Berea sandstone conducted by *Lockner et al.* [1992] could be simulated and results compared. Full three-dimensional models could be created and more particles could be used to get higher-resolution results. The fractal nature of cracking in actual rocks could be simulated by specifying a fractal distribution of particle sizes [see *Morgan and Boettcher*, 1999]. Finally, if low numerical damping was used, then seismic source information (such as magnitude and mechanism) could be determined for every modeled crack [see *Hazzard et al.*, 1998].

Acknowledgments. A special thank you to David Potyondy, Mark Board, and Peter Cundall at Itasca Consulting Group for all of their help with the modeling. This work would also have not been possible without the financial assistance of the Committee of Vice Chancellors and Principals of the universities of the U.K. for providing James Hazzard with an Overseas Research Scholarship.

References

Antonellini, M. A., and D. D. Pollard, Distinct element modeling of deformation bands in sandstone, *J. Struct. Geol.*, *17*, 1165–1182, 1995.

Blair, S. C., and N. G. W. Cook, Analysis of compressive fracture in rock using statistical techniques, part I, A non-linear rule-based model, *Int. J Rock Mech. Min. Sci. Geomech. Abstr.*, *35*, 837–848, 1998.

Brace, W. F., and E. G. Bombolakis, A note on brittle crack growth in compression, *J. Geophys. Res.*, *68*, 3709–3713, 1963.

Brace, W. F., B. W. Paulding, and C. Scholz, Dilatancy in the fracture of crystalline rocks, *J. Geophys. Res.*, *71*, 3939–3953, 1966.

Cundall, P. A., Numerical experiments on localization in frictional materials, *Ing. Arch.*, *59*, 148–159, 1989.

Cundall, P. A., Numerical modelling of jointed and faulted rock, in *Mechanics of Jointed and Faulted Rock*, pp. 11–18, A. A. Balkema, Brookfield, Vt., 1990.

Cundall, P. A., and O. Strack, A discrete element model for granular assemblies, *Geotechnique*, *29*(1), 47–65, 1979.

Deresiewicz, H., Mechanics of granular matter, in *Advances in Applied Mechanics*, vol. 5, edited by H. L. Dryden et al., pp. 233–306, Academic, San Diego, Calif., 1958.

Donzé, F., S. A. Magnier, and J. Bouchez, Numerical modeling of a highly explosive source in an elastic-brittle rock mass, *J. Geophys. Res.*, *101*, 3103–3112, 1996.

Feustel, A. J., Seismic attenuation in underground mines: Measurement techniques and applications to site characterization, Ph.D. thesis, Queen's Univ., Kingston, Ont., Canada, 1995.

Harris, R. A., and S. M. Day, Dynamics of fault interaction: parallel strike-slip faults, *J. Geophys. Res.*, *98*, 4461–4472, 1993.

Hazzard, J. F., Numerical modelling of acoustic emissions and dynamic rock behaviour, Ph.D. thesis, Keele Univ., Keele, England, 1998.

Hazzard, J. F., S. C. Maxwell, and R. P. Young, Micromechanical modelling of acoustic emissions, in *Eurock 98*, pp. 519–526, Soc. of Pet. Eng., Inc., Trondheim, Norway, 1998.

Hildyard, M. W., A. Daehnke, and P. A. Cundall, WAVE: A computer program for investigating elastodynamic issues in mining, *Proc. U.S. Symp. Rock Mech.*, *35th*, 519–524, 1995.

Hill, D. P., et al., Seismicity remotely triggered by the magnitude 7.3 Landers, California, earthquake, *Science*, *260*, 1617–1623, 1993.

Horii, H., and S. Nemat-Nasser, Compression-induced microcrack growth in brittle solids: Axial splitting and shear failure, *J. Geophys. Res.*, *90*, 3105–3125, 1985.

Kelly, D., D. C. Peck, and R. S. James, Petrography of granitic rock samples from the 420 level of the Underground Research Laboratory, Pinawa, Manitoba. Laurentian Univ., Sudbury, Ont., Canada, 1993.

Kemeny, J. M., A model for non-linear rock deformation under compression due to sub-critical crack growth, *Int. J. Rock Mech. Min. Sci. Geomech. Abstr.*, *28*, 459–467, 1991.

Leddra, M. J., M. E. Jones, and A. S. Goldsmith, Laboratory investigation of the compaction of chalk under conditions of increasing effective stress, paper presented at Third North Sea Chalk Symposium, Norw. Pet. Dir. Copenhagen, 1990.

Lockner, D. A., Rock failure, in *Rock Physics and Phase Relations*, edited by T. J. Ahrens, pp. 127–147, AGU, Washington, D. C., 1995.

Lockner, D. A., and T. R. Madden, A multiple-crack model of brittle fracture, 1, Non-time-dependent simulations, *J. Geophys. Res.*, *96*, 19,623–19,642, 1991.

Lockner, D. A., J. D. Byerlee, V. Kuksenko, A. Ponomarev, and A. Sidorin, Quasi-static fault growth and shear fracture energy in granite, *Nature*, *350*(7), 39–42, 1991.

Lockner, D. A., J. D. Byerlee, V. Kuksenko, A. Ponomarev, and A. Sidorin, Observations of quasi-static fault growth from acoustic emissions, in *Fault Mechanics and Transport Properties of Rocks*, edited by B. Evans and T. Wong, pp. 3–32, Academic, San Diego, Calif., 1992.

Malan, D. F., and J. A. L. Napier, Computer modelling of granular material microfracturing, *Tectonophysics*, *248*, 21–37, 1995.

Martin, C. D., Strength of massive Lac du Bonnet granite around underground openings, Ph.D. thesis, Univ. of Manitoba, Winnipeg, Canada, 1993.

Menendez, B., W. Zhu, and T. Wong, Micromechanics of brittle faulting and cataclastic flow in Berea sandstone, *J. Struct. Geol.*, *18*, 1–16, 1996.

Moore, D. E., and D. A. Lockner, The role of microcracking in shear-fracture propagation in granite, *J. Struct. Geol.*, *17*, 95–114, 1995.

Mora, P., and D. Place, Numerical simulation of earthquake faults with gouge: Toward a comprehensive explanation for the heat flow paradox, *J. Geophys. Res.*, *103*, 21,067–21,089, 1998.

Morgan, J., and M. S. Boettcher, Numerical simulations of granular shear zones using the distinct element method, 1, Shear zone kine-

matics and the micromechanics of localization, *J Geophys. Res.*, *104*, 2703–2719, 1999.

Okui, Y., and H. Horii, A micromechanics-based continuum theory for microcracking localization of rocks under compression, in *Continuum Models for Materials with Microstructure*, edited by H.-B. Mühlhaus, pp. 27–68, John Wiley, New York, 1995.

Potyondy, D. O., and P. A. Cundall, Modeling notch-formation mechanisms in the URL mine-by test tunnel using bonded assemblies of circular particles, *Int J. Rock Mech. Min. Sci.*, *35*, paper 067, 1998.

Potyondy, D., and P. Cundall, Modeling of notch formation in the URL mine-by tunnel, Phase IV, Enhancements to the PFC model of rock, report to Atomic Energy of Canada Limited, *Ont. Hydro Nucl. Waste Manage. Div. Rep. 06819-REP-01200-10002-R00*, Itasca Consult. Group, Minneapolis, Minn., 1999.

Potyondy, D. O., P. A. Cundall, and C. Lee, Modeling of rock using bonded assemblies of circular particles, in *Second North American Rock Mechanics Symposium—NARMS '96*, edited by M. Aubertin, pp. 1934–1944, A. A. Balkema, Brookfield, Vt., 1996.

Read, R. S., and C. D. Martin, Monitoring the excavation-induced response of granite, *Proc. U.S. Symp. on Rock Mechanics*, *33rd*, 201–210, 1992.

Reches, Z., and D. A. Lockner, Nucleation and growth of faults in brittle rocks, *J. Geophys. Res.*, *99*, 18,159–18,173, 1994.

Salamon, M. D. G., Keynote address: Some applications of geomechanical modelling in rockburst and related research, in *3rd International Symposium on Rockbursts and Seismicity in Mines*, edited by R. P. Young, pp. 297–310, A. A. Balkema, Brookfield, Vt., 1993.

Sammis, C. G., and M. F. Ashby, The failure of brittle porous solids under compressive stress states, *Acta Metall.*, *34*(3), 511–526, 1986.

Scholz, C. H., Microfracturing and the inelastic deformation of rock in compression, *J. Geophys. Res.*, *73*, 1414–1432, 1968.

Scholz, C. H., L. R. Sykes, and Y. P. Aggarwal, Earthquake prediction: A physical basis, *Science*, *181*, 803–810, 1973.

Tapponnier, P., and W. F. Brace, Development of stress-induced microcracks in Westerly granite, *Int. J. Rock Mech. Min. Sci. Abstr.*, *13*, 103–112, 1976.

Wong, T., C. David, and W. Zhu, The transition from brittle faulting to cataclastic flow in porous sandstones: Mechanical deformation, *J. Geophys. Res.*, *102*, 3009–3025, 1997.

J. F. Hazzard and R. P. Young, Department of Earth Sciences, University of Liverpool, 4 Brownlow St., Liverpool L69 7GP, England, U.K. (hazzard@liv.ac.uk; r.p.young@liv.ac.uk)

S. C. Maxwell, ESG Canada Inc., 1 Hyperion Court, Kingston, Ontario, Canada K7K 7G3. (s.c.maxwell@esg.ca)

(Received February 24, 1999; revised January 17, 2000; accepted March 13, 2000.)